

SCIENTIFIC REPORTS

OPEN

Bolometric photodetection using plasmon-assisted resistivity change in vanadium dioxide

Hironobu Takeya¹, James Frame², Takuo Tanaka^{3,4,5,6}, Yoshiro Urade⁷, Xu Fang² & Wakana Kubo^{1,3}

Vanadium oxide is a key sensing material for bolometric photodetection, thanks to its strong temperature dependence of resistivity close to room temperature. Here we demonstrate the photodetection of a stoichiometric vanadium dioxide thin film integrated with silver nanorods. The nanorods convert light into heat, consequently suppressing the resistivity of vanadium dioxide via localised surface plasmon resonance. Incorporation of this thermo-plasmonic effect into bolometric photodetection allows for wavelength and polarisation sensitivity. This work opens the path to a broad family of photodetection functionalities for vanadium dioxide-based microbolometers.

Bolometric photodetection utilises the dependence of material resistivity on temperature to detect light. Due to its unique properties such as extremely broadband response and high sensitivity, it is chosen for many applications including uncooled infrared imaging and single photon detection^{1–3}. At present, vanadium oxide is the most widely used sensing material in microbolometers⁴. Several unique properties of the material have led to its market dominance, including strong light absorption and an orders-of-magnitude change in resistivity (i.e. a high temperature coefficient of resistance) close to room temperature⁵.

Among the various phases of vanadium oxide, stoichiometric vanadium dioxide (VO₂) is frequently chosen for proof-of-principle demonstrations, as its simple composition allows for high reproducibility of experimental results^{6–8}. An emerging research topic of VO₂ is its interplay with surface plasmons^{9–15}. Previous work has found that plasmonic resonances can facilitate the phase change of VO₂ and the phase change can in turn modulate plasmonic resonances¹⁶. Most of this research has been conducted in the context of tuneable plasmonic devices and reconfigurable metamaterials. In contrast, this work focuses on utilising plasmons to introduce new functionalities (here wavelength and polarisation sensitivity) to bolometric photodetection. As far as we know, this is the first report on the electrical detection of light via plasmonic resonances in VO₂. Compared to plasmon-assisted photodetection on other material platforms¹⁷, our choice of VO₂ lends our work immediate relevance to practical applications. In particular, although VO₂-based photodetection lacks several functionalities available in 2D materials (e.g. ultrafast photodetection in graphene¹⁸), its mature technology platform is ideal for testing the integration of sensing materials and novel plasmonic nanostructures.

Figure 1(a) schematically illustrates the sample and its measurement configuration. The sample consisted of a thin layer of VO₂ prepared by magnetron sputtering on a bulk sapphire (Al₂O₃) substrate. Two rectangular silver (Ag) electrodes were subsequently grown on the sample surface using thermal evaporation. The high quality of the VO₂ film was verified by measuring the dc resistivity between the electrodes in a thermal cycle (Fig. 1(b)). The resistivity changed by over three orders of magnitude between 20 °C and 100 °C, and showed a phase transition temperature, defined as the centre of the resistivity hysteresis loop, of ~68 °C.

¹Division of Advanced Electrical and Electronics Engineering, Tokyo University of Agriculture and Technology, 2-24-16 Naka-cho, Koganei-shi, Tokyo, 184-8588, Japan. ²School of Electronics and Computer Science, University of Southampton, Southampton, SO17 1BJ, UK. ³Metamaterials Laboratory, RIKEN Cluster for Pioneering Research, 2-1, Hirosawa, Wako, Saitama, 351-0198, Japan. ⁴Department of Physics, Faculty of Science, Gakushuin University, 1-5-1 Mejiro, Toshima-ku, Tokyo, 171-8588, Japan. ⁵Innovative Photon Manipulation Research Team, RIKEN Center for Advanced Photonics, 2-1 Hirosawa, Wako, Saitama, 351-0198, Japan. ⁶Department of Chemical Science and Engineering Major in Chemical Science and Engineering, School of Materials and Chemical Technology, Tokyo Institute of Technology, 4259 Nagatsuta-cho, Midori-ku, Yokohama, Kanagawa, 226-8503, Japan. ⁷Department of Electronic Science and Engineering, Kyoto University, Kyoto, 615-8510, Japan. Correspondence and requests for materials should be addressed to X.F. (email: x.fang@soton.ac.uk) or W.K. (email: w-kubo@cc.tuat.ac.jp)

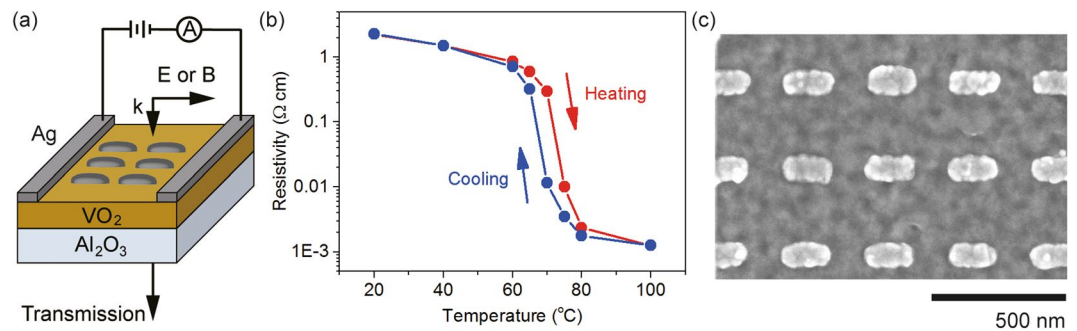


Figure 1. VO₂ bolometer integrated with silver (Ag) nanorods. (a) Schematic of the sample and its measurement configuration. The sample consists of two Ag electrodes and an array of Ag nanorods on top of a VO₂ film, which is supported by a bulk Al₂O₃ substrate. The nanorods are illuminated by light linearly polarised along either their short or long axis. The temperature is controlled and monitored using a Peltier element and a temperature sensor (not depicted). (b) Resistivity hysteresis loop measured between the two electrodes before the fabrication of nanorods. (c) SEM images of a section of the nanorod array.

A periodic array of Ag nanorods was subsequently patterned between the two electrodes following a standard electron beam lithography and lift-off process. The array was 1.8 mm × 1.8 mm in size and was located at the middle of the two electrodes. The nanorods had a thickness of 40 nm, averaged planar dimensions of 95 nm × 180 nm and a periodicity of 300 nm × 300 nm (Fig. 1(c)). Ag was chosen as the nanorod material for these two reasons. (1) Ag has extremely low resistivity ($1.6 \times 10^{-6} \Omega \cdot \text{cm}$ at 20 °C) compared to VO₂ (measured as 2.3 Ω·cm at 20 °C), making a small change in the VO₂ relatively easy to detect. (2) Ag supports strong localised surface plasmon resonance (LSPR) within the entire wavelength range of interest, thus enabling investigation of the thermo-plasmonic effect.

The VO₂-nanorod sample obtained after nanofabrication was characterised using two home-built systems. System A consisted of an optical microscope (Olympus BX51) and a fibre-coupled spectrometer (Ocean Optics HR4000) for measuring the transmission. Meanwhile, System B consisted of a Xenon lamp (Hamamatsu Photonics E7536) and a monochromator (Shimadzu SPG-120S) for measuring the dc resistivity under light illumination. In both systems, the nanorods were illuminated at normal incidence, with the light linearly polarised along either their long or short axis. The light was focused to the centre of the array, and the focal spot was slightly smaller than the array. The temperature of the sample was maintained at 66 °C, a value slightly below the phase transition temperature, for transition-edge detection. This temperature control was achieved by using a Peltier module, which was attached to the bottom of the Al₂O₃ substrate and a temperature sensor, which was placed at the surface of the VO₂ film close to the nanorod array.

Figure 2(a) shows the transmission spectrum of the sample measured using System A, where the intensity of incident light was kept at a very low level to minimise any thermal effect. The incident light was polarised along the short axis of the nanorods. A plain area of the same VO₂ film was used as reference. The spectrum shows a strong and broad feature at 650 nm corresponding to a ~30% drop in transmission compared to transmission at 900 nm and 400 nm. Figure 2(a) also shows the resistivity measured using System B, where the sample was illuminated by light narrow in spectral width (~46 nm in full-width at half-maximum) and high in intensity (~10 mW·cm⁻²). The central wavelength of the incident light was tuned from 450 nm to 850 nm at a step of 100 nm, with the resistivity between the two electrodes measured at each wavelength. As VO₂ has very small thermal conductivity ($6 \text{ W} \cdot \text{m}^{-1} \cdot \text{K}^{-1}$)¹⁹, the nanorod array could drift in temperature with time under light illumination. To minimise such influence on the resistivity measurement, the whole wavelength range was swept four times; Fig. 2(a) shows the average and standard error of these four measurements.

The resistivity in Fig. 2(a) is wavelength dependent, and it roughly correlates with the transmission. Both values are smallest at 650 nm and largest at ~450 nm. To interpret this correlation, the electromagnetic behaviour of the sample is numerically simulated using a 3D finite-element solver (COMSOL Multiphysics). The nanorod is treated as a hemi-spherocylinder with dimensions taken from experimental values. The wavelength dependent permittivity of Ag and Al₂O₃ is taken from refs^{20,21}, respectively. The permittivity of VO₂, which depends on both the wavelength and metallic volume fraction (i.e. the filling factor of metallic phase in a dielectric matrix)²², is taken from ref.²³. The volume fraction is set as 0.8 for the best fitting to experiment, and its influence on the transmission spectrum is shown in Fig. S2.

Figure 2(b) shows the numerically simulated transmission spectrum, which reproduces the experimental result reasonably well. High-order diffraction in the forward direction is observed for wavelengths below 530 nm. The zero-order spectrum corresponds to the measured spectrum due to the large distance between the sample and detector in the experiment. Compared to experiment, the simulated spectrum shows a redshift of ~50 nm, which is attributed to the difference in nanorod dimensions and material permittivity between the experiment and simulation (see Supplementary Information for details^{24,25}). Figures 2(c,d) show the electromagnetic near-field distribution at respectively 700 nm, the wavelength with the smallest transmission in simulation, and 450 nm, the shortest wavelength for resistivity measurement. At 700 nm, the nanorod shows strong and highly confined enhancement of electromagnetic field. The electric field increases by a factor of ~6.5 compared to the

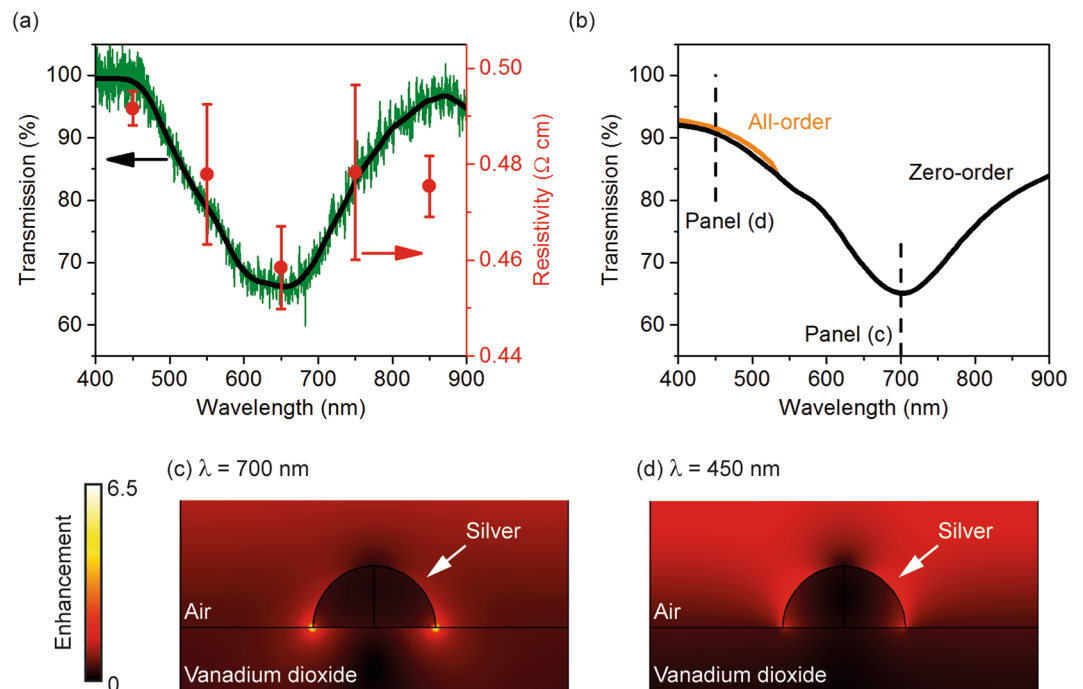


Figure 2. Optical and optoelectronic properties of the sample. **(a)** Experimentally measured optical transmission and wavelength dependent resistivity of the sample. The incident light is polarised along the short axis of the nanorods. The green and the black line are the measured and smoothed spectra, respectively. **(b)** Numerically simulated transmission of the sample. High-order forward diffraction is observed at wavelengths below 530 nm. **(c,d)** Electric field distribution at a 2D plane bisecting a nanorod along the short axis at a wavelength of **(c)** 700 nm and **(d)** 450 nm. The enhancement factor is with respect to the incident field.

incident light; this level of enhancement is only observed at the two sharp edges of the nanorod. These characteristics indicate that the broad and strong transmission feature is induced by the LSPR of the nanorods. The LSPR is significantly less pronounced at 450 nm as both the enhancement and confinement are much weaker (Fig. 2(d)). Figures 2(b,c) show that transmission amplitude directly reflects LSPR strength, with low transmission corresponding to strong LSPR.

We consequently attribute the correlation between transmission and resistivity in Fig. 2(a) to the thermo-plasmonic effect. Plasmonic nanostructures are well-known for their high efficiency in converting electromagnetic energy to thermal energy. Although considered as a key limiting factor for many applications, this effect has found several applications including reconfigurable metamaterials, heat-assisted magnetic recording, photothermal therapy, plasmon-assisted chemistry and plasmon-enhanced optical trapping^{26–29}. For our sample, conversion of light to heat is most efficient at the LSPR resonance wavelength (650 nm in experiment and 700 nm in simulation). The nanorod array is at a slightly higher temperature than the temperature sensor nearby³⁰, and the VO₂ beneath the array is slightly suppressed in resistivity. For wavelengths far away from the resonance wavelength, the heating effect induced by the array is smaller, and the suppression in the resistivity is also smaller.

In addition to the wavelength dependence shown in Fig. 2, we further explored the polarisation dependence of the sample. Figure 3 shows corresponding results at the orthogonal light polarisation, i.e. the incident light is polarised along the long axis of the nanorods. The optical transmission shows two pronounced features at ~550 nm and ~850 nm, while the resistivity only traces the feature at ~850 nm (Fig. 3(a)). This difference originates from the different nature of the two spectral features: only the one at ~850 nm is induced by LSPR. This is supported by the near-field distribution in Fig. 3(c,d), where strong LSPR is only visible at 850 nm. The spectral feature at ~550 nm in Fig. 3(a), although not faithfully reproduced in simulation in Fig. 3(b), becomes more pronounced at smaller metallic volume fractions (Fig. S2). It is consequently attributed to the interplay between high-order diffraction and multiple interference inside the VO₂ layer, as both phenomena depend on the permittivity of VO₂, which in turn depends on the volume fraction. As this feature is not related to any near-field enhancement, no obvious suppression of resistivity is observed at this wavelength.

The difference between Figs 2 and 3 clearly shows the influence of plasmonic resonance on photodetection. The wavelength dependent resistivity in both figures, however, shows a relatively large standard error. Although a detailed discussion is beyond the scope of this proof-of-principle demonstration, we have noticed in ongoing experiments that covering the Ag nanorods with a thin layer of magnesium fluoride may significantly reduce the standard error. The cover layer is expected to protect the nanorods from tarnishing, as well as to stabilise the temperature distribution at the edges of the nanorods by reducing the influence of air convection. Rigorous experimental investigation and theoretical analysis of the optical, thermal and electrical behaviours of the device at the nanoscale will lead to higher device sensitivity.

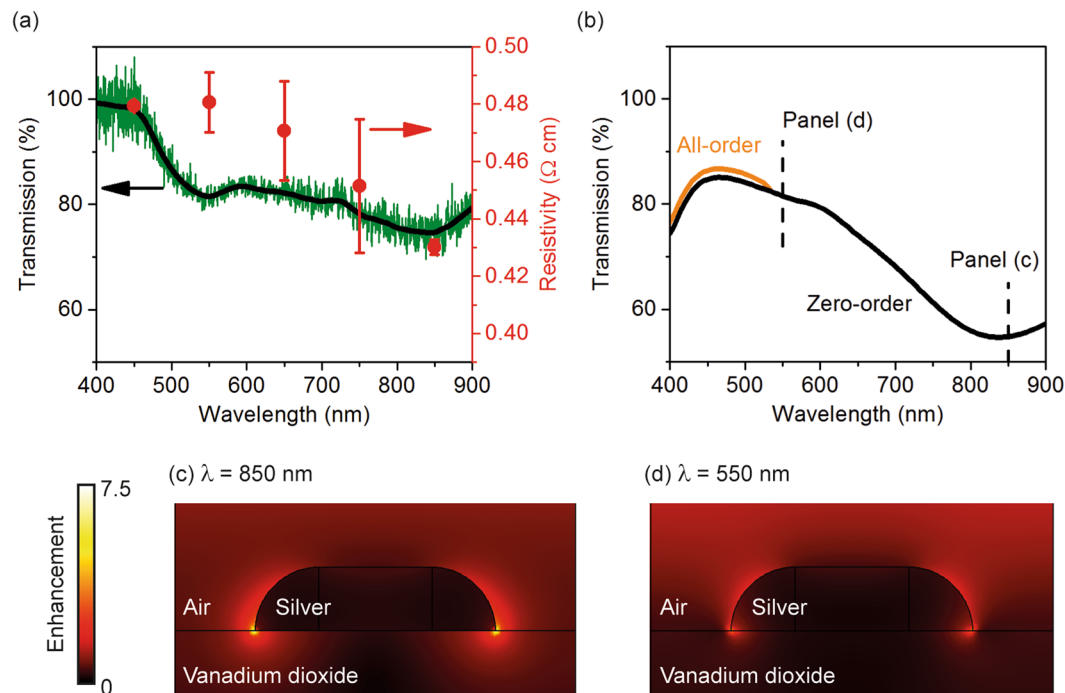


Figure 3. Sample properties under long-axis light excitation. **(a)** Experimental optical transmission and electrical resistivity. The green and the black line are the measured and smoothed spectra, respectively. The incident light is polarised along the long axis of the nanorods. **(b)** Numerically simulated transmission of the sample. **(c,d)** Electric field distribution at a 2D plane bisecting a nanorod along the long axis at a wavelength of **(c)** 850 nm and **(d)** 550 nm.

To conclude, we have demonstrated bolometric photodetection using plasmon-assisted resistivity change in VO_2 . Ag plasmonic nanostructures grown on top of the VO_2 film increase heat generation via the excitation of LSPR and consequently suppress its resistivity. This change in resistivity depends on the strength of the LSPR, which can be tuned by controlling the wavelength and polarisation of incident light. A rough and simple correlation between transmission and resistivity is observed for spectral features induced by LSPR. The nanorod array introduces a certain degree of wavelength and polarisation sensitivity to bolometric photodetection. As plasmonic nanostructures can facilitate advanced control over light, this work can lead to the development of multi-functional, VO_2 -based plasmonic microbolometers.

Methods

Sample fabrication. The sample consisted of a thin layer of VO_2 (250 nm thick) on top of a bulk sapphire (Al_2O_3 , ~1 mm thick) substrate. The VO_2 layer was fabricated via reactive magnetron sputtering of vanadium under continuous flow of argon and oxygen gases (temperature = 450 °C, RF power = 200 W, Ar flow rate = 130 sccm, O_2 flow rate = 3 sccm, total gas pressure = 0.5 Pa, and total sputtering time \approx 2 hours). Two rectangular silver (Ag) electrodes were fabricated on the sample surface by thermal evaporation. These electrodes were 100 nm in thickness, 7.5 mm in length, and separated by 2.0 mm in between. A periodic array of Ag nanorods was patterned between the two electrodes following a standard electron beam lithography (JEOL JBX-6300FS) and lift-off process.

Data availability. The data from this paper can be obtained from the University of Southampton ePrints research repository: <https://doi.org/10.5258/SOTON/D0615>.

References

- Hadfield, R. H. Single-photon detectors for optical quantum information applications. *Nat Photonics* **3**, 696–705, <https://doi.org/10.1038/nphoton.2009.230> (2009).
- Eisaman, M. D., Fan, J., Migdall, A. & Polyakov, S. V. Invited Review Article: Single-photon sources and detectors. *Rev Sci Instrum* **82**, 071101, <https://doi.org/10.1063/1.3610677> (2011).
- Walcott, T. M. *Bolometers: theory, types and applications*. (Nova Science Publishers, 2011).
- Rogalski, A. Recent progress in infrared detector technologies. *Infrared Phys Techn* **54**, 136–154, <https://doi.org/10.1016/j.infrared.2010.12.003> (2011).
- Gurvitch, M., Luryi, S., Polyakov, A. & Shabalov, A. Nonhysteretic behavior inside the hysteresis loop of VO_2 and its possible application in infrared imaging. *J Appl Phys* **106**, 104504, <https://doi.org/10.1063/1.3243286> (2009).
- Wu, J. M. & Chang, W. E. Ultrahigh Responsivity and External Quantum Efficiency of an Ultraviolet-Light Photodetector Based on a Single VO_2 Microwire. *Acs Appl Mater Inter* **6**, 14286–14292, <https://doi.org/10.1021/am503598g> (2014).
- Joushaghani, A. *et al.* Wavelength-size hybrid Si- VO_2 waveguide electroabsorption optical switches and photodetectors. *Opt Express* **23**, 3657–3668, <https://doi.org/10.1364/Oe.23.003657> (2015).

8. Fan, L. L. *et al.* Infrared Response and Optoelectronic Memory Device Fabrication Based on Epitaxial VO₂ Film. *ACS Appl Mater Inter* **8**, 32971–32977, <https://doi.org/10.1021/acsami.6b12831> (2016).
9. Kats, M. A. *et al.* Vanadium Dioxide as a Natural Disordered Metamaterial: Perfect Thermal Emission and Large Broadband Negative Differential Thermal Emittance. *Phys Rev X* **3**, 041004, <https://doi.org/10.1103/PhysRevX.3.041004> (2013).
10. Kim, J. T. CMOS-compatible hybrid plasmonic modulator based on vanadium dioxide insulator-metal phase transition. *Opt Lett* **39**, 3997–4000, <https://doi.org/10.1364/Ol.39.003997> (2014).
11. Liu, L., Kang, L., Mayer, T. S. & Werner, D. H. Hybrid metamaterials for electrically triggered multifunctional control. *Nat Commun* **7**, 13236, <https://doi.org/10.1038/ncomms13236> (2016).
12. Hashemi, M. R. M., Yang, S. H., Wang, T. Y., Sepulveda, N. & Jarrahi, M. Electronically-Controlled Beam-Steering through Vanadium Dioxide Metasurfaces. *Sci Rep-Uk* **6**, 35439, <https://doi.org/10.1038/srep35439> (2016).
13. Urade, Y. *et al.* Dynamically Babinet-invertible metasurface: a capacitive-inductive reconfigurable filter for terahertz waves using vanadium-dioxide metal-insulator transition. *Opt Express* **24**, 4405–4410, <https://doi.org/10.1364/Oe.24.004405> (2016).
14. Li, Z. *et al.* Tunable mid-infrared patch antennas based on VO₂ phase transition. *J Mod Optic* **64**, 1762–1767, <https://doi.org/10.1080/009500340.2017.1314030> (2017).
15. Zhu, Z. H., Evans, P. G., Haglund, R. F. & Valentine, J. G. Dynamically Reconfigurable Metadevice Employing Nanostructured Phase-Change Materials. *Nano Lett* **17**, 4881–4885, <https://doi.org/10.1021/acs.nanolett.7b01767> (2017).
16. Liu, H. W., Lu, J. P. & Wang, X. R. Metamaterials based on the phase transition of VO₂. *Nanotechnology* **29**, 024002, <https://doi.org/10.1088/1361-6528/aa9cb1> (2018).
17. Koppens, F. H. L. *et al.* Photodetectors based on graphene, other two-dimensional materials and hybrid systems. *Nat Nanotechnol* **9**, 780–793, <https://doi.org/10.1038/Nnano.2014.215> (2014).
18. Tielrooij, K. J. *et al.* Generation of photovoltage in graphene on a femtosecond timescale through efficient carrier heating. *Nat Nanotechnol* **10**, 437–443, <https://doi.org/10.1038/Nnano.2015.54> (2015).
19. Samsonov, G. V. *The oxide handbook*. (Springer, 2013).
20. Yang, H. H. U. *et al.* Optical dielectric function of silver. *Phys Rev B* **91**, 235137, <https://doi.org/10.1103/PhysRevB.91.235137> (2015).
21. Pirozhenko, I. & Lambrecht, A. Influence of slab thickness on the Casimir force. *Phys Rev A* **77**, 013811, <https://doi.org/10.1103/PhysRevA.77.013811> (2008).
22. Qazilbash, M. M. *et al.* Mott transition in VO₂ revealed by infrared spectroscopy and nano-imaging. *Science* **318**, 1750–1753, <https://doi.org/10.1126/science.1150124> (2007).
23. Hatef, A., Zamani, N. & Johnston, W. Coherent control of optical absorption and the energy transfer pathway of an infrared quantum dot hybridized with a VO₂ nanoparticle. *J Phys-Condens Mat* **29**, 155305, <https://doi.org/10.1088/1361-648X/aa61ee> (2017).
24. Fang, X., Tseng, M. L., Tsai, D. P. & Zheludev, N. I. Coherent Excitation-Selective Spectroscopy of Multipole Resonances. *Phys Rev Appl* **5**, 014010, <https://doi.org/10.1103/PhysRevApplied.5.014010> (2016).
25. Fang, X., MacDonald, K. F., Plum, E. & Zheludev, N. I. Coherent control of light-matter interactions in polarization standing waves. *Sci Rep-Uk* **6**, 31141, <https://doi.org/10.1038/srep31141> (2016).
26. Baffou, G. & Quidant, R. Thermo-plasmonics: using metallic nanostructures as nano-sources of heat. *Laser Photonics Rev* **7**, 171–187, <https://doi.org/10.1002/lpor.201200003> (2013).
27. Zhou, N. *et al.* Plasmonic near-field transducer for heat-assisted magnetic recording. *Nanophotonics-Berlin* **3**, 141–155, <https://doi.org/10.1515/nanoph-2014-0001> (2014).
28. Wang, S. H. *et al.* Plasmonic Copper Sulfide Nanocrystals Exhibiting Near-Infrared Photothermal and Photodynamic Therapeutic Effects. *ACS Nano* **9**, 1788–1800, <https://doi.org/10.1021/nn506687t> (2015).
29. Ndukaife, J. C. *et al.* Long-range and rapid transport of individual nano-objects by a hybrid electrothermoplasmonic nanotweezer. *Nat Nanotechnol* **11**, 53, <https://doi.org/10.1038/Nnano.2015.248> (2016).
30. Baffou, G. *et al.* Photoinduced Heating of Nanoparticle Arrays. *ACS Nano* **7**, 6478–6488, <https://doi.org/10.1021/nn401924n> (2013).

Acknowledgements

The authors are grateful to Dr. Masao Kitano and Dr. Toshihiro Nakanishi for providing VO₂ samples, and Dr. Nicolas Green for fruitful discussions. This work was supported by JSPS Grant-in-Aid for Exploratory Research (15K13266), the Royal Society (RG170314), the Daiwa Anglo-Japanese Foundation (Daiwa Foundation Award 5453/12324), and JSPS Core-to-core program. The VO₂ film was fabricated with the help of Kyoto University Nano Technology Hub, as part of the Nanotechnology Platform Project sponsored by MEXT in Japan.

Author Contributions

W.K. conceived the idea of this study. H.T. performed the measurements with support from T.T. Y.U. fabricated the VO₂ film. J.F. and X.F. conducted the numerical simulations. H.T., X.F. and W.K. wrote the manuscript. All authors contributed to the analysis and interpretation of results. W.K. and X.F. supervised and coordinated all the work.

Additional Information

Supplementary information accompanies this paper at <https://doi.org/10.1038/s41598-018-30944-2>.

Competing Interests: The authors declare no competing interests.

Publisher's note: Springer Nature remains neutral with regard to jurisdictional claims in published maps and institutional affiliations.



Open Access This article is licensed under a Creative Commons Attribution 4.0 International License, which permits use, sharing, adaptation, distribution and reproduction in any medium or format, as long as you give appropriate credit to the original author(s) and the source, provide a link to the Creative Commons license, and indicate if changes were made. The images or other third party material in this article are included in the article's Creative Commons license, unless indicated otherwise in a credit line to the material. If material is not included in the article's Creative Commons license and your intended use is not permitted by statutory regulation or exceeds the permitted use, you will need to obtain permission directly from the copyright holder. To view a copy of this license, visit <http://creativecommons.org/licenses/by/4.0/>.

© The Author(s) 2018